Journal of Southeast University (English Edition) Vol. 34, No. 2, pp. 229 - 236 June 2018 ISSN 1003—7985

Damage process and performance of PVA fiber-reinforced alkali-activated slag mortar plate under bending

Dong Chenghao[1] Li Tao[1] Zhang Yamei[1] Liu Jiaping[2]

([1]School of Materials Science and Engineering, Southeast University, Nanjing 211189, China)

([2]Jiangsu Key Laboratory of Construction Materials, Southeast University, Nanjing 211189, China)

Abstract: The effects of unoiled polyvinyl alcohol (PVA) fiber with four different volume fractions of 0%, 1.0%, 1.5% and 2.0% on the bending properties of alkali-activated slag (AAS) mortar plates were studied. Meanwhile, the acoustic emission (AE) technique and a high-speed camera were utilized to detect the crack development over the complete damage process, and the scanning electronic microscopy (SEM) was used to observe the fiber-matrix interface. Test results show that PVA fibers play a significant role in the toughness improvement of AAS plates. However, the enhancing effect of PVA fibers on the bending behaviour of AAS plates at 120 d is not as remarkable as at early ages. It is observed that the failure process of the PVA fiber-reinforced alkali-activated slag plate can be divided into three stages: elastic stage, main crack formation stage and post-peak load stage. Observations on the fracture surface of specimens indicate that the deterioration process of specimens under bending changed from fiber pull-out at 3 and 28 d to fiber fracture at 120 d.

Key words: alkali-activated slag; polyvinyl alcohol fiber; bend; acoustic emission; damage process

DOI: 10.3969/j.issn.1003-7985.2018.02.013

Over the past decades, alkali-activated materials, especially alkali-activated slag, have attracted a great interest throughout the world due to their numerous advantages like low energy consumption[1], low greenhouse gas emission[2], high early mechanical properties[3], strong aggregate-matrix interface[4-5], resistance to chemical attack[6-7] and high reduction in chloride diffusion[8].

Plain alkali-activated material is a brittle material with low tensile strength. This undesired behaviour can be improved by inclusion of short discrete fibers to control the initiation and propagation of cracks[9-10]. The incorporation of fibers in AAS materials can substantially improve their engineering properties such as tensile strength, flexural strength, shrinkage behaviour, resistance to fatigue, impact, and thermal shock[11-12]. Partial replacement of slag with metakaolin also brings positive effects to the properties of the AAS system, such as prolongation of setting time and enhancement of strength[11, 13].

The performance of fiber-reinforced composites depends on the properties of matrix, fibers, and most important, the bond between fibers and the matrix. In PVA fiber-reinforced cementitious composites, such as engineered cementitious composites (ECC) invented by Li et al.[14-15], the key factors affecting the composite are the aspect ratio, dosage of fibers and the bonding between fibers and the matrix[16]. However, there are few references concerning the influence of the PVA fiber on the mechanical properties and damage process of alkali-activated slag mortar, especially at later ages. Lee et al.[17] investigated slag-based alkali-activated mortar at 28 d reinforced by the oiled PVA fiber and achieved the feasibility of attaining tensile strain up to 4.7%. Natali et al.[18] modified some properties of alkali-activated ladle-slag at 7 d by employing PVA fibers, and the enhancement in ductility after the first crack load was obvious. Zhang et al.[19-20] investigated the behaviour of the short PVA fiber-reinforced fly ash-metakaolin geopolymer boards at 28 d. Their conclusion demonstrated that the incorporation of high-volume PVA fibers changed the impact failure mode of geopolymer boards from a brittle to ductile pattern.

AE technique has been used to monitor the initiation and propagation of cracks in cement-based composites[21] and fiber-reinforced concretes[22-25]. The commonly used parameters of AE technique are AE hit, amplitude and energy[26]. The amplitude is defined at the peak of the signal. The area under the envelope of the AE event is defined as the absolute energy. The real-time change of flaws is indicated by the activity degree of AE signals which are expressed by the cumulative number of AE hits that exceed the threshold limit. An AE hit can be directly related to micro-cracking, and a sudden increase in cumulative hits is usually related to the formation of macro-cracking[27]. However, the use of the parameter "hits" only provides an indication of the number of "events" and does not quantify the magnitude of the acoustic events[22]. The intensity of AE signals is expressed by the character-

Received 2017-10-21, **Revised** 2018-01-17.

Biographies: Dong Chenghao (1994—), male, graduate; Zhang Yamei (corresponding author), female, doctor, professor, ymzhang@seu.edu.cn.

Foundation items: The National Basic Research Program of China (973 Program) (No. 2015CB655100), the National Natural Science Foundation of China (No. 51378115).

Citation: Dong Chenghao, Li Tao, Zhang Yamei, et al. Damage process and performance of PVA fiber-reinforced alkali-activated slag mortar plate under bending[J]. Journal of Southeast University (English Edition), 2018, 34(2): 229 - 236. DOI: 10.3969/j.issn.1003-7985.2018.02.013.

istic parameters of amplitude and absolute energy. The large amplitude indicates the great degree of damage, while small amplitude corresponds to the initiation or propagation of micro cracks[27-28]. The major AE waves of high absolute energy are generally assessed to indicate the formation of large fracture surfaces, such as macro cracks[27, 29].

In the light of the above mentioned facts, the aim of this study is to improve the bending properties of AAS mortar by the addition of low-price unoiled PVA fiber, and to detect the damage process and failure characteristics of PVA fiber-reinforced AAS mortar plates at a long curing age via utilizing the AE system. The effects of curing age and fiber dosage on the mechanical properties have also been investigated. As a result, the failure process of fiber-reinforced alkali-activated slag plates are revealed.

1 Experiment

1.1 Raw materials

Ground granulated blast furnace slag and metakaolin are used as binding materials in this investigation. The chemical compositions of the slag and metakaolin used are presented in Tab. 1. The specific gravity of slag and metakaolin are 2.84 and 2.1 g/cm^3, respectively. The blaine specific surface area and the average particle diameter of slag are 436 m^2/kg and 11.86 μm, respectively. Industrial grade sodium hydroxide and industrial grade water glass are used. Water glass has a SiO_2 content of 30.94 % and a Na_2O content of 10.76%. The silicate modulus M_s is 2.97.

Natural river sand with a maximum size of 0.6 mm is utilized as fine aggregate. The length and density of unoiled PVA fiber are 12 mm and 1.2 g/cm^3, respectively. The aspect ratio (length/diameter), tensile strength and elastic modulus of the PVA fiber are 390, 1 350 MPa and 30.6 GPa, respectively. In general, the properties of unoiled PVA fiber are similar to those of the oiled PVA fiber, and the cost of the former is approximately 1/8 of the latter. However, the unoiled PVA fiber may be ruptured in a cementitious matrix due to its strong frictional and chemical bonding to cement hydrates[30].

Tab. 1 Chemical composition of slag and metakaolin in mass fraction %

Composition content	$w(SiO_2)$	$w(Al_2O_3)$	$w(CaO)$	$w(MgO)$	$w(Na_2O)$	$w(Fe_2O_3)$	$w(P_2O_5)$	$w(SO_3)$	$w(TiO_2)$
Slag	33.13	15.44	34.23	7.40	1.50	0.22	4.55	2.53	0.53
Metakaolin	51.46	43.11	0.22	1.66	1.73	0.50	0.36	0.03	0.82

1.2 Mix design and sample preparation

The binder is composed of 10% metakaolin and 90% slag. Sodium hydroxide and sodium silicate are mixed to provide a SiO_2/Na_2O molar ratio of 1.5 and the Na_2O content of 5% of the binder. The alkali solution is prepared and cooled in advance. The water/binder ratio and the aggregate/binder ratio of all the mixtures are kept constant at 0.4 and 1.5, respectively. The volume fractions of the PVA fiber are 1.0%, 1.5%, and 2%. Plain specimens without fibers are cast for comparison purpose.

Initially, binder and aggregate are dry-mixed for one minute and then fibers are gradually added by hands before the alkali solution is gradually added. The mixing procedure lasts for about 3 min. After being cast into steel molds (20 mm × 60 mm × 360 mm), fresh mixtures are kept in a humid chamber ((20 ± 1) ℃ and 90% relative humidity) for one or two days until demolded, and then cured in the same chamber up to 3, 28, 60 and 120 d.

1.3 Test methodologies

The flow tests were performed to evaluate the workability of fresh mixtures according to GB/T 2419—2005. Instron 8802 machine was used to conduct four-point bending tests. The displacement control mode at a loading rate of 0.5 mm/min was applied. The clear distance between supports was 320 mm and the mid-span was 106.7 mm. The geometry of the test specimen and the test setup are shown in Fig. 1.

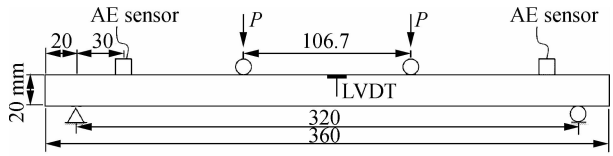

Fig. 1 A schematic view of a four-point bending test (unit: mm)

During the bending test, the displacement at the center of specimens was measured by two linear variable differential transformers (LVDTs) fixed in the middle of both sides of the specimen. Meanwhile, a PIC-2 system and a camera were used, respectively, to collect AE signals and record the crack development at a frequency of one photo per second. Two resonant sensors (type R15) with a center frequency of 150 kHz were attached by Vaseline on the top surface of specimens. The parameters for AE test, as shown in Tab. 2, are determined according to Ref. [29].

Tab. 2 Parameters of AE tests

Parameter	Threshold/dB	Pre-amp gain/dB	Filter/kHz	PDT/μs	HDT/μs	HLT/μs
Value	40	40	20 to 400	50	200	300

2 Results and Discussion

2.1 Workability

The flow diameters of all fresh mixtures are given in Fig. 2. With the increase of the fiber volume V_f from 0 to 2%, a gradual decrease in the flow diameter of alkali-activated slag mortars was observed. From Fig. 3, it can be seen that the distribution of PVA fibers in mortars incorporated with high volume fraction fibers was not as uniform as in plain and low volume fiber included ones.

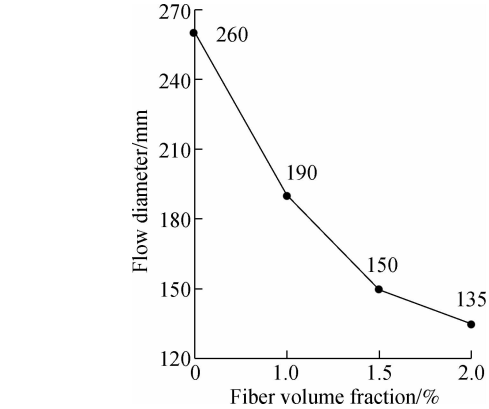

Fig. 2 Influence of fiber volume fraction on flow diameter

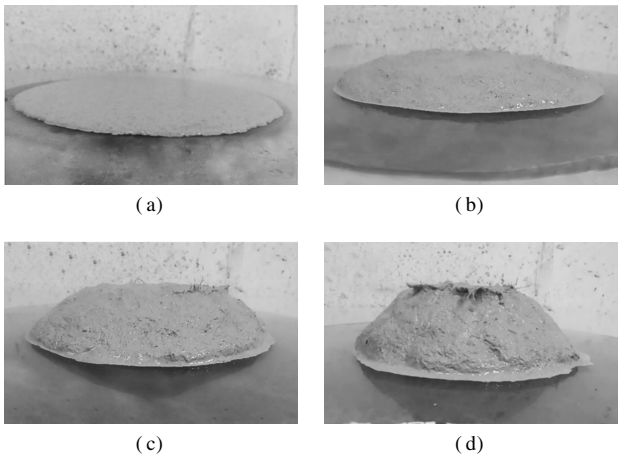

Fig. 3 Influence of fiber volume fraction on workability of mortar. (a) $V_f = 0$; (b) $V_f = 1.0\%$; (c) $V_f = 1.5\%$; (d) $V_f = 2.0\%$

2.2 Behaviour of mortars under four-point bending

The load-displacement curves of specimens with different PVA fiber contents at different ages under four-point bending are shown in Fig. 4. These curves, selected from three replicated specimens of each group, represent the closest one to the average mechanical performance. Generally, all the reference specimens without fibers exhibited a typical brittle failure, although the maximum load capacity increased with the increase in curing age. At 3 d, the strain-hardening behaviour was found in all PVA fiber-reinforced specimens. At 28 d, the overall loading capacity increased; however, the strain-hardening behaviour was weakened. At 120 d, the strain-hardening stage became very short, while the loading capacity increased. After the ultimate load, the pull-out stages of the PVA fibers in the specimens cured for 3, 28, and 60 d were observed, although these stages became shorter with the increasing curing age. At 120 d, two typical peaks appeared on the load-displacement curves. The first peak was correlated to the crack of the AAS matrix. With the cracking of the matrix, the loading capacity dropped suddenly. Meanwhile, with the transferring of load from the cracked matrix to fibers, the loading capacity began to increase again until the second peak load where the fracture of fibers occurred, and thereafter, the loading capacity dropped quickly until the failure of the specimen.

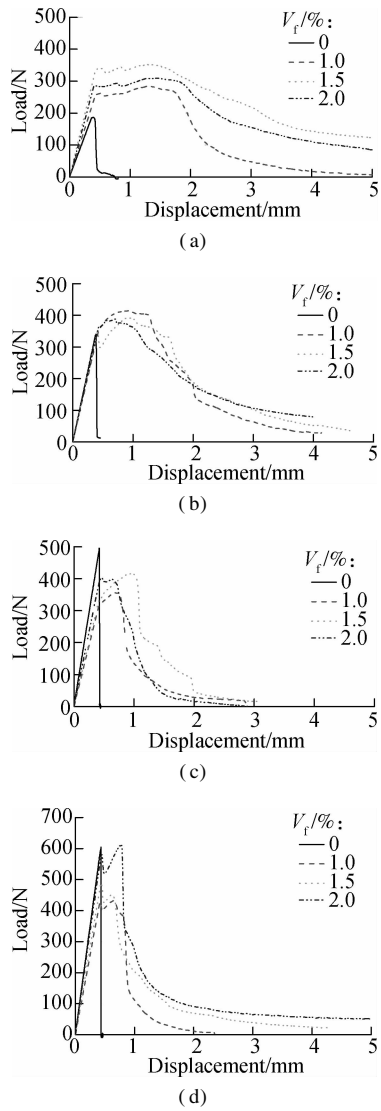

Fig. 4 Load-displacement curves of AAS mortar specimens with different fiber contents. (a) 3 d; (b) 28 d; (c) 60 d; (d) 120 d

The average flexural strength, the displacement at ultimate load, the toughness and the elastic modulus of three tested specimens are shown in Tab. 3. The modulus of elasticity in bending of AAS mortar was calculated according to ASTM D6272—17. The toughness was calculated by integrating the area till 3 mm[31] in the load-dis-

Tab. 3 Flexural strength, displacement, toughness and elastic modulus of AAS mortar specimens

Age/d	Flexural strength/MPa				Displacement at peak load/mm				Toughness/(N·mm)				Elastic modulus/GPa
	V_f = 0	V_f = 1.0%	V_f = 1.5%	V_f = 2.0%	V_f = 0	V_f = 1.0%	V_f = 1.5%	V_f = 2.0%	V_f = 0	V_f = 1.0%	V_f = 1.5%	V_f = 2.0%	V_f = 0
3	3.6	5.3	5.9	5.6	0.32	1.56	1.70	1.12	57.9	693.2	915.9	715.7	15.2
28	6.2	6.7	6.9	6.7	0.38	0.67	0.96	0.72	77.9	763.5	706.5	653.1	20.3
60	7.7	5.8	7.1	6.6	0.41	0.55	0.99	0.81	99.9	321.2	657.6	421.7	23.1
120	9.0	7.3	7.6	9.7	0.41	0.61	0.63	0.55	115.1	380.3	587.2	618.8	27.4

placement curves. It can be seen that the flexural strength, the displacement at the ultimate load and the toughness of specimens with PVA fibers at 3 d were greatly enhanced, compared with those of specimens without PVA fibers. At a later age, though the flexural strength of specimens was not strongly affected by the addition of PVA fibers, the displacement and the toughness were much obviously improved by the incorporation of PVA fibers as well. Even if the displacement and the toughness gradually decreased with the increase in curing age, the toughness of specimens at 120 d with PVA fibers was still much higher than that of specimens without fibers.

2.3 Microstructure of specimens at different curing ages

The decrease of displacement and toughness of PVA fiber-reinforced AAS mortars at later age can be explained by the change of the their microstructure. First, the continuous hydration of AAS matrix densified the microstructure of the mortar. Secondly, the bonding between PVA fibers and matrix became stronger with the increase in curing time. This change of microstructure also led to the the deterioration process of specimens changing from fiber pull-out to fiber pull-off. As shown in Fig. 5, the fracture surface of the specimen at 3 d was porous and rough with relatively long pulled-out PVA fibers. At 120 d, the fracture surface became dense and relatively flat with much fewer and smaller pores and shorter fractured PVA fibers. From Fig. 6, it can be seen that the surface of the PVA fiber in the 120 d specimen was covered with dense AAS hydration products, indicating the strong bonding between the fiber and matrix. The reduction of toughness caused by the increase of curing age is analogous to the effect caused by the decrease of water/cement ratio, which also leads to the compactness of the matrix of PVA fiber-reinforced cementitious composites[32].

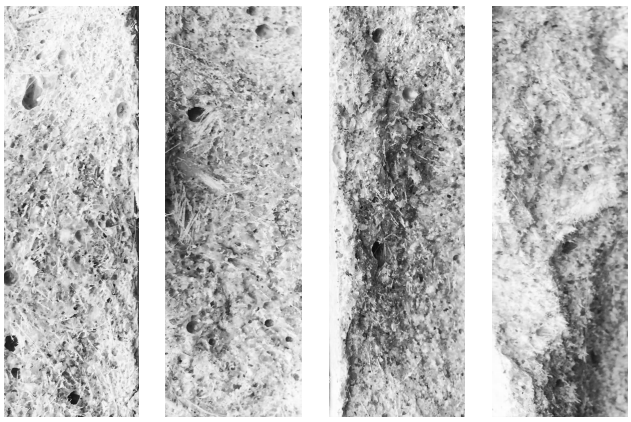

(a) (b) (c) (d)

Fig. 5 Fracture surface of specimens with $V_f = 2.0\%$ fibers at different ages. (a) 3 d; (b) 28 d; (c) 60 d; (d) 120 d

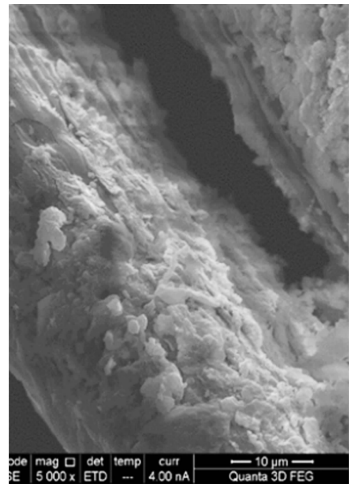

Fig. 6 SEM micrograph of PVA fiber and matrix from 120 d specimens

The modulus of elasticity in bending of AAS mortar increased continuously from 15.2 GPa at 3 d to 27.4 GPa at 120 d. However, the elastic modulus of the PAV fiber was only 30.6 GPa. Therefore, the ultimate loading capacity of PVA fiber-reinforced specimens at 120 d cannot be improved as significantly as those at 3 d. Generally, a higher volume fraction of fibers in the matrix can result in better performance; i. e., higher loading capacity and better toughness but only if fibers can be uniformly distributed in the matrix. From Tab. 3, however, the influence of the dosage of PVA fibers on the performance of specimens was scattering, since unoiled PVA fibers tended to "bundle" in the matrix when the fiber content increased, and the "bundle" of fibers caused more flaws in the matrix, leading to the decline of mechanical strength[30].

2.4 Damage process monitored by AE technique

AE signals together with load-time curves of specimens are shown in Figs. 7 and 8. For the specimens without PVA fibers, the development of cumulative hits can be divided into two typical stages. During the first stage, the cumulative hits kept at a very low level till the end of the corresponding linear stage. After the first stage, cumula-

tive hits increased quickly in a short time, and the amplitude and the energy of AE signals also became significantly strong until the failure of the specimen. Meanwhile, the cracks rapidly propagated at this stage. Compared with the 120 d specimen, the cumulative hits and the amplitude of the signals of the 28 d specimen during the first stage were much higher.

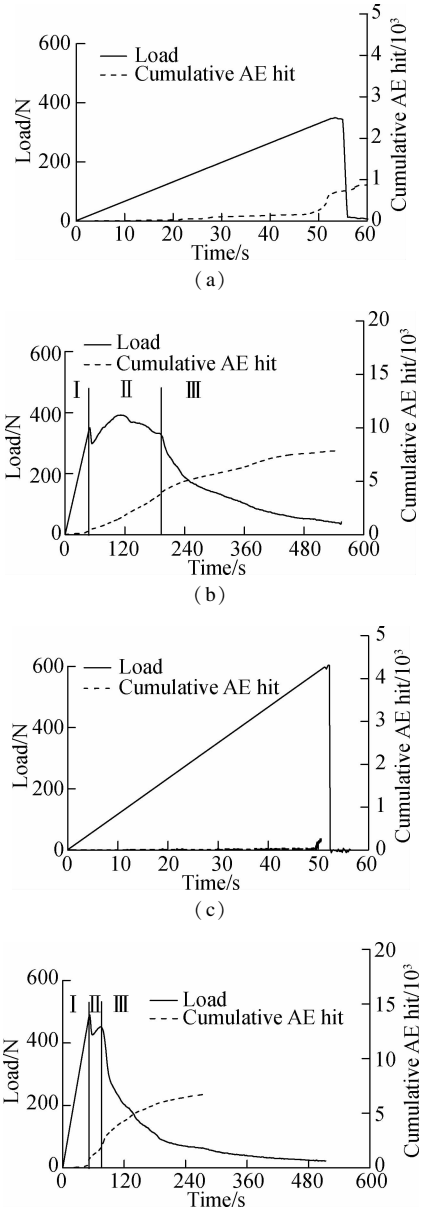

Fig. 7 The cumulative AE hits of AAS plates. (a) V_f =0 at 28 d; (b) V_f =1.5% at 28 d; (c) V_f =0 at 120 d; (d) V_f =1.5% at 120 d

Consistent with Ref. [33], the cracking process of PVA fiber-reinforced alkali-activated slag mortar plates under bending can be classified into three typical stages, i. e., the elastic stage (Ⅰ), the main crack formation stage (Ⅱ) and the post-peak stage (Ⅲ). As shown in Figs. 7(b) and (d), during the elastic stage, the cumulative AE hits grew slowly since there was less damage at this stage. Following this stage, a significant increase of the cumulative AE hit was observed. During the second stage, crack propagation was impeded due to the bridging effect of PVA fibers[16,32]. Along with the generation and propagation of new micro-cracks and the continuous stress transferring from matrix to fibers, cumulative AE hit grew rapidly and continuously till a macro crack was formed. This supported the opinion of Alam et al.[27] that a sudden increase in hits was related to macro cracking. After the macro crack was formed, the loading capacity of the specimen began to drop. At the final stage, fibers were either gradually pulled out or fractured and the macroscopic crack propagated to the top of the specimen. Meanwhile, the increase of the cumulative hit

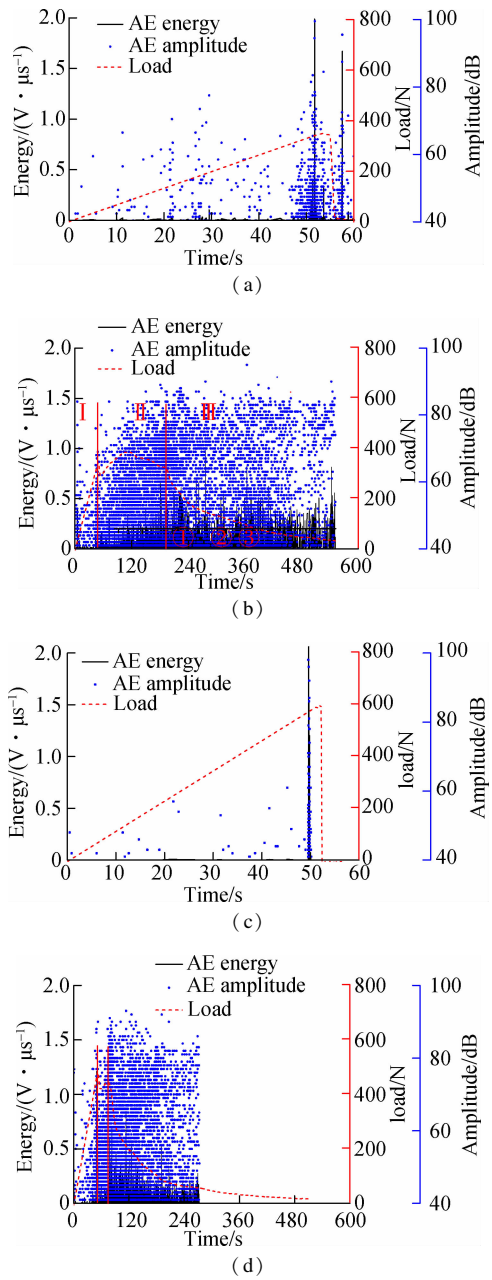

Fig. 8 Absolute energy and amplitude of AE signals of AAS plates. (a) V_f =0 at 28 d; (b) V_f =1.5% at 28 d; (c) V_f =0 at 120 d; (d) V_f =1.5% at 120 d

number of AE signals slowed down since the damage only concentrated at a localized zone with few new cracks. With the increase of curing age from 28 to 120 d, both stage Ⅱ and stage Ⅲ became shorter, although the corresponding load was higher, which coincided well with the decrease of the toughness with the curing age in Tab. 3.

Fig. 9 presents the photos taken by the high-speed camera under different loading times of the specimen in Fig. 7 (b). From Figs. 9(a) and (b), it can be clearly seen that the appearance of the initial crack was at 49 s and the visible main crack at 113 s. The results match well with the end of elastic stage and the end of the main crack formation stage.

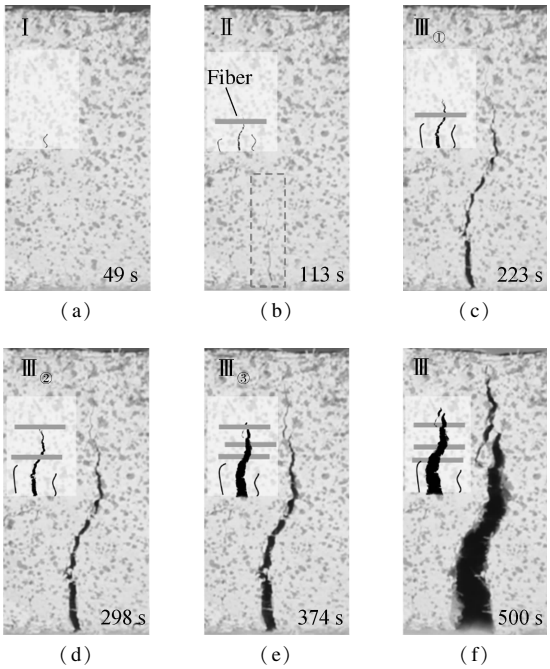

Fig. 9 Cracks at different loading times of specimen with V_f = 1.5% at 28 d. (a) Initial cracking of matrix; (b) Cracking arrested by fibers; (c) Fibers bridging cracks; (d) Cracking arrested by fibers again; (e) Previously bridged fibers fractured and cracking arrested by fibers ahead crack tip; (f) Fibers fractured

The increase of absolute energy at main crack formation stage Ⅱ is due to the formation of micro cracks at closer intervals of time[28] during the transferring of the load from matrix to fibers. It is worth noting from Fig. 8 (b) that high-energy signals mainly concentrate in stage Ⅲ, rather than in stage Ⅱ, where the external loading is higher and many micro cracks are generated. It should also be noted that the signals in the middle part of stage Ⅲ are sparser. As shown in Figs. 8(b) and 9, stage Ⅲ can be further divided into three sub-stages by AE absolute energy, i. e. peak Ⅲ①, valley Ⅲ② and peak Ⅲ③. As shown in Fig. 9(c), the main crack developed significantly during the first high energy stage Ⅲ① between 180 and 240 s. This high energy phase was related to the extension of micro cracks across fibers and then coalescing into a macro crack in a localized zone. This process definitely caused the rapid drop of loading capacity as well. Other studies indicate that crack extension through the coarse aggregate will also emit many high absolute energy signals[23]. In the middle "valley" stage Ⅲ②, the further propagation of crack tips was arrested by fibers lying ahead (see Fig. 9(d)), thereby requiring a cumulative driving force to further propagate. Fewer strong signals were generated during this phase. Kim et al.[22] reported that the discrete jumps in the energy release in the fiber-reinforced specimen can be explained in part by the fibers acting to arrest cracks before they propagated across the specimen. The second peak Ⅲ③ can be related to the pull-out or fracture of fibers across cracks (see Fig. 9(e)) that generated high energy AE signals. Wu et al.[23] also reported that very high amplitude signals emitted by specimens near failure were generated by pull-out and breakage of fibers. Finally, the macro crack propagated to the top (see Fig. 9(f)). Investigation on concrete by AE technique[21,27] showed that the absolute energy AE signals presented two peaks and a softening phase between the two peaks during the post-peak loading stage. Alam et al.[21,27] reported that the two peaks were related to micro cracking and macro cracking, respectively, and that the softening phase was due to the interlock or shielding of aggregate in front of the notch.

From Fig. 8(d), it can be seen that the energy of AE signals at the post-peak load stage of specimen at 120 d is relatively lower than that in Fig. 8(b). This is due to the dense structure of the matrix and the strong bond between matrix and fibers which leads to the fracture rather than pull-out of most of the PVA fibers. Due to the very strong bond, it is possible that the signals generated during the pull-out process of PVA fibers from AAS matrix are stronger than those produced when PVA fibers are broken.

3 Conclusions

1) Fiber inclusion influenced the bending behaviour of AAS mortar plates dramatically. All of the PVA fiber-reinforced alkali-activated slag mortar plates exhibited strain-hardening performance, although the increase in fiber content did not show positive effect on enhancing the matrix due to the undesirable distribution state of fibers in matrix. With the increase of curing duration from 3 to 120 d, the toughening effect of the PVA fiber on the AAS matrix was weakened gradually.

2) The deterioration process of specimens under bending changed from fiber pull-out at early ages to fracture at later ages due to the gradually increased bond between PVA fibers and the AAS matrix.

3) The cumulative hits, the amplitude and the absolute energy of AE signals can be used to reveal the damage process of specimens under bending. The failure process of the PVA fiber-reinforced alkali-activated slag mortar

plate can be divided into three stages: the elastic stage, the main crack formation stage and the post-peak load stage. The absolute energy signals of the post-peak stage of 28 d PVA fiber-reinforced AAS mortar can be further divided into three sub-stages, i. e. the peak, valley and peak stages.

4) The energy of AE signals at the post-peak load stage of specimens at 120 d was relatively lower than that at 28 d due to the dense structure of the matrix and the strong bond between matrix and fibers which led to the fracture rather than pull-out of most of the PVA fibers.

References

[1] Li Z, Ding Z, Zhang Y. Development of sustainable cementitious materials [C]//*Proceedings of International Workshop on Sustainable Development and Concrete Technology*. Beijing, China, 2004: 55 - 76. (in Chinese)

[2] Davidovits J. Geopolymer chemistry and properties [C]//*Proceedings of the* 1*st European Conference on Soft Mineralurgy*. Compiegne, France, 1998: 25 - 48.

[3] Fernández-Jiménez A, Palomo J G, Puertas F. Alkali-activated slag mortars: Mechanical strength behaviour [J]. *Cement and Concrete Research*, 1999, **29**(8): 1313 - 1321. DOI: 10.1016/s0008-8846(99)00154-4.

[4] Shi C, Xie P. Interface between cement paste and quartz sand in alkali-activated slag mortars [J]. *Cement and Concrete Research*, 1998, **28**(6): 887 - 896. DOI: 10.1016/S0008-8846(98)00050-7.

[5] Brough A R, Atkinson A. Automated identification of the aggregate-paste interfacial transition zone in mortars of silica sand with Portland or alkali-activated slag cement paste [J]. *Cement and Concrete Research*, 2000, **30**(6): 849 - 854. DOI: 10.1016/S0008-8846(00)00254-4.

[6] Komljenović M, Baščarević Z, Marjanović N, et al. External sulfate attack on alkali-activated slag [J]. *Construction and Building Materials*, 2013, **49**: 31 - 39. DOI: 10.1016/j. conbuildmat. 2013. 08. 013.

[7] Lee N K, Lee H K. Influence of the slag content on the chloride and sulfuric acid resistances of alkali-activated fly ash/slag paste [J]. *Cement and Concrete Composites*, 2016, **72**: 168 - 179. DOI: 10. 1016/j. cemconcomp. 2016. 06. 004.

[8] Roy D M, Jiang W, Silsbee M R. Chloride diffusion in ordinary, blended, and alkali-activated cement pastes and its relation to other properties [J]. *Cement and Concrete Research*, 2000, **30**(12): 1879 - 1884. DOI: 10. 1016/S0008-8846(00)00406-3.

[9] Provis J L, Deventer J S J V. *Alkali activated materials* [M]. The Netherlands: Springer, 2014.

[10] Hannant D J. *Fibre cements and fibre concretes* [M]. Mineralogical Society, 1978.

[11] Rashad A M. A comprehensive overview about the influence of different additives on the properties of alkali-activated slag-A guide for civil engineer [J]. *Construction and Building Materials*, 2013, **47**: 29 - 55. DOI: 10. 1016/j. conbuildmat. 2013. 04. 011.

[12] Rashad A M. A comprehensive overview about the influence of different admixtures and additives on the properties of alkali-activated fly ash [J]. *Materials and Design*, 2014, **53**: 1005 - 1025. DOI: 10. 1016/j. matdes. 2013. 07. 074.

[13] Borges P H R, Banthia N, Alcamand H A, et al. Performance of blended metakaolin/blastfurnace slag alkali-activated mortars [J]. *Cement and Concrete Composites*, 2016, **71**: 42 - 52. DOI: 10. 1016/j. cemconcomp. 2016. 04. 008.

[14] Li V C, Leung C K Y. Steady-state and multiple cracking of short random fiber composites [J]. *Journal of Engineering Mechanics*, 1992, **118**(11): 2246 - 2264.

[15] Maalej M, Li V C. Introduction of strain hardening engineered cementitious composites in design of reinforced concrete flexural members for improved durability [J]. *ACI Structural Journal*, 1995, **92**(2): 167 - 176. DOI: 10. 14359/1150.

[16] Said S H, Razak H A, Othman I. Flexural behavior of engineered cementitious composite (ECC) slabs with polyvinyl alcohol fibers [J]. *Construction and Building Materials*, 2015, **75**: 176 - 188. DOI: 10. 1016/j. conbuildmat. 2014. 10. 036.

[17] Lee B Y, Cho C G, Lim H J, et al. Strain hardening fiber-reinforced alkali-activated mortar—A feasibility study [J]. *Construction and Building Materials*, 2012, **37**: 15 - 20. DOI: 10. 1016/j. conbuildmat. 2012. 06. 007.

[18] Natali A, Manzi S, Bignozzi M C. Novel fiber-reinforced composite materials based on sustainable geopolymer matrix [J]. *Procedia Engineering*, 2011, **21**: 1124 - 1131. DOI: 10. 1016/j. proeng. 2011. 11. 2120.

[19] Zhang Y, Wei S, Li Z, et al. Impact properties of geopolymer based extrudates incorporated with fly ash and PVA short fiber [J]. *Construction and Building Materials*, 2008, **22**(3): 370 - 383.

[20] Zhang Y, Wei S, Li Z, et al. Geopolymer extruded composites with incorporated fly ash and polyvinyl alcohol short fiber [J]. *ACI Materials Journal*, 2009, **106**(1): 3 - 10. DOI: 10. 1016/j. conbuildmat. 2006. 08. 006.

[21] Alam S Y, Saliba J, Loukili A. Fracture examination in concrete through combined digital image correlation and acoustic emission techniques [J]. *Construction and Building Materials*, 2014, **69**: 232 - 242. DOI: 10. 1016/j. conbuildmat. 2014. 07. 044.

[22] Kim B, Weiss W J. Using acoustic emission to quantify damage in restrained fiber-reinforced cement mortars [J]. *Cement and Concrete Research*, 2003, **33**(2): 207 - 214. DOI: 10. 1016/S0008-8846(02)00978-X.

[23] Wu K, Chen B, Yao W. Study on the AE characteristics of fracture process of mortar, concrete and steel-fiber-reinforced concrete beams [J]. *Cement and Concrete Research*, 2000, **30**(9): 1495 - 1500. DOI: 10. 1016/S0008-8846(00)00358-6.

[24] Soulioti D, Barkoula N M, Paipetis A, et al. Acoustic emission behavior of steel fibre reinforced concrete under bending [J]. *Construction and Building Materials*, 2009, **23**(12): 3532 - 3536. DOI: 10. 1016/j. conbuildmat. 2009. 06. 042.

[25] Aggelis D G, Soulioti D V, Sapouridis N, et al. Acoustic

emission characterization of the fracture process in fibre reinforced concrete[J]. *Construction and Building Materials*, 2011, **25**(11):4126-4131. DOI:10.1016/j.conbuildmat.2011.04.049.

[26] Huang M, Jiang L T, Liaw P, et al. Using acoustic emission in fatigue and fracture materials research[J]. *JOM*, 1998, **50**(11):1-14.

[27] Alam S Y, Loukili A, Grondin F, et al. Use of the digital image correlation and acoustic emission technique to study the effect of structural size on cracking of reinforced concrete[J]. *Engineering Fracture Mechanics*, 2015, **143**:17-31. DOI:10.1016/j.engfracmech.2015.06.038.

[28] Muralidhara S, Prasad B K R, Eskandari H, et al. Fracture process zone size and true fracture energy of concrete using acoustic emission[J]. *Construction and Building Materials*, 2010, **24**(4):479-486. DOI:10.1016/j.conbuildmat.2009.10.014.

[29] Wang C, Zhang Y, Ma A. Investigation into thefatigue damage process of rubberized concrete and plain concrete by AE analysis[J]. *Journal of Materials in Civil Engineering*, 2011, **23**(7):953-960. DOI:10.1061/(ASCE)MT.1943-5533.0000257.

[30] Pan Z, Wu C, Liu J, et al. Study on mechanical properties of cost-effective polyvinyl alcohol engineered cementitious composites (PVA-ECC)[J]. *Construction and Building Materials*, 2015, **78**:397-404. DOI:10.1016/j.conbuildmat.2014.12.071.

[31] Aydın S, Baradan B. The effect of fiber properties on high performance alkali-activated slag/silica fume mortars[J]. *Composites Part B: Engineering*, 2013, **45**(1):63-69. DOI:10.1016/j.compositesb.2012.09.080.

[32] Niu H, Wu W, Xing Y, et al. Effects of water/cement ratio on properties and microstructure of PVA fiber-reinforced cementitious composites[J]. *Fuhe Cailiao Xuebao/Acta Materiae Compositae Sinica*, 2015, **32**(4):1067-1074. DOI:10.13801/j.cnki.fhclxb.20141031.002. (in Chinese)

[33] Aggelis D G. Classification of cracking mode in concrete by acoustic emission parameters[J]. *Mechanics Research Communications*, 2011, **38**(3):153-157. DOI:10.1016/j.mechrescom.2011.03.007.

PVA 纤维增强碱激发矿渣砂浆板弯曲性能和破坏过程

董承浩[1] 李 涛[1] 张亚梅[1] 刘加平[2]

([1] 东南大学材料科学与工程学院, 南京 211189)

([2] 东南大学江苏省土木工程材料重点实验室, 南京 211189)

摘要:研究了掺入体积掺量为1.0%、1.5%和2.0% 未经油化处理的聚乙烯醇(PVA)纤维对碱激发矿渣砂浆板弯曲性能的影响. 同时,利用声发射(AE)系统监测破坏过程中裂缝的发展状况,利用扫描电镜(SEM)观测纤维-基体界面. 研究结果表明,PVA 纤维对碱激发矿渣砂浆起到了较大的增韧作用,但对120 d 砂浆板的弯曲强度的提升效果不如早期明显. PVA 纤维增强碱激发矿渣试件破坏过程可分为弹性阶段、主裂缝形成阶段和极限荷载后3个阶段. 观察发现, 抗弯荷载下3和28 d龄期样品中的纤维以拔出为主,而120 d样品中的纤维则是拔断破坏.

关键词:碱激发矿渣;PVA 纤维;弯曲;声发射;破坏过程

中图分类号:TU528.572